Magnetic ordering in $Er_3Cu_4X_4$ (X = Si, Ge, Sn)

D H Ryan[1]**, J M Cadogan**[2]**, R Gagnon**[1] **and I P Swainson**[3]

[1] Physics Department and Centre for the Physics of Materials, McGill University,
3600 University Street, Montreal, QC, H3A 2T8, Canada
[2] School of Physics, The University of New South Wales, Sydney, NSW 2052, Australia
[3] Neutron Programme for Materials Research, Steacie Institute for Molecular Sciences,
National Research Council, Chalk River Laboratories, ON, K0J 1J0, Canada

Abstract
Magnetic ordering of the orthorhombic $Er_3Cu_4X_4$ (X = Si, Ge, Sn) system has been studied using both ^{119}Sn and ^{166}Er Mössbauer spectroscopy, combined with neutron diffraction. We observe two distinct ordering events for the erbium moments on the 2d and 4e sites (T_N (Er 2d) > T_N (Er 4e)) and confirm that the Er 2d moments are larger than those on the Er 4e site. Comparison of neutron diffraction with ^{166}Er Mössbauer spectroscopy shows that the ordering of the Er 4e moments is far from complete, even at 0.7 T_N, causing neutron diffraction analysis to severely underestimate the Er 4e moments in the $Er_3Cu_4X_4$ system.

1. Introduction

The orthorhombic $R_3Cu_4X_4$ (X = Si, Ge, Sn) alloy system has attracted significant attention recently [1–3] and has been found to exhibit a complex variety of magnetic ordering behaviour depending on both the rare-earth (R) and metalloid (X) present in the alloy. The rare-earth atoms occupy two crystallographically distinct sites in these compounds (4e and 2d), and the moments observed at the two sites are generally quite different from each other and greatly reduced from their free-ion values [1, 3–5]. For the Tb and Er germanides [3] and the Er stannide [1] the two rare-earth sites even order at very different temperatures. Of these alloys, those with Er present the most extreme deviations from simple behaviour with transition temperatures for the Er 2d site being about twice that on the Er 4e site, and ordered moment ratios (μ_{2d}/μ_{4e}) of nearly three in the germanide [3] and four in the stannide [1].

We present here an extensive study of the $Er_3Cu_4X_4$ (X = Si, Ge, Sn) alloy system using both bulk and microscopic probes of the magnetic ordering. ^{119}Sn Mössbauer spectroscopy is used to look for separate ordering of the Er 2d and Er 4e sites through the transferred hyperfine fields at the two Sn sites in the stannide (4f and 4h) which have quite different Er coordinations. ^{166}Er Mössbauer spectroscopy provides a direct measurement of the erbium moments at both Er crystallographic sites in all three alloys, and has been shown to yield perfect agreement

Table 1. Lattice parameters and unit cell volumes for $Er_3Cu_4X_4$ derived from analysis of Cu Kα x-ray diffraction data. Also given are the results of Curie–Weiss fits (θ_p and $p_{\text{eff}} = g[J(J+1)]^{\frac{1}{2}}$) to the χ_{ac} data in figures 1–3.

	$Er_3Cu_4Si_4$	$Er_3Cu_4Ge_4$	$Er_3Cu_4Sn_4$
a (Å)	13.588(3)	13.799(4)	14.546(8)
b (Å)	6.513(2)	6.610(2)	6.903(4)
c (Å)	4.097(1)	4.153(1)	4.408(2)
vol (Å^3)	362.6(2)	378.8(2)	442.6(4)
θ_p (K)	−6.4(2)	−9.4(2)	−5.6(1)
p_{eff} (μ_B)	10.3(1)	11.2(1)	10.4(1)

with neutron diffraction derived moments in Er_3Ge_4 [6]. Finally, we have carried out neutron diffraction measurements on the silicide at temperatures from ambient down to 2.4 K in order to follow the ordering behaviour and the temperature dependence of the ordered moments on the two Er sites in some detail. We confirm the separation of ordering temperatures at the two Er sites; however, both the neutron diffraction and ^{166}Er Mössbauer spectroscopy data show that the reported Er 4e moments are far too small, with the correct μ_{2d}/μ_{4e} moment ratio ranging from 1.28(1) in the silicide to *equal* in the stannide.

2. Sample preparation and basic characterization

Samples were prepared in a tri-arc furnace with a base pressure of better than 6×10^{-7} mbar. Stoichiometric amounts of the pure elements (Er (99.9%), Cu (99.99%), Si (99.9999%), Ge (99.999%) and Sn (99.99%)) were melted several times under pure (<1 ppm impurity) argon to ensure homogeneity. The ingots were then annealed under vacuum at 800 °C for two weeks and water quenched.

Powder x-ray diffraction measurements were made at ambient temperature using Cu Kα radiation and analysed using GSAS/EXPGUI [7] to extract lattice parameters and check for impurities. Analysis confirms that the samples were primarily composed of the orthorhombic $R_3Cu_4X_4$ phase, (Gd$_3$Cu$_4$Ge$_4$-type, *Immm* space group, No. 71 [8]). The $R_3Cu_4X_4$ structure has two Er sites (2d and 4e), one Cu site (8n) and two X sites (4f and 4h). Atomic positions were not refined in the analysis of the x-ray data. Lattice parameters of the $R_3Cu_4X_4$ phases are given in table 1. The samples also contained less than 2 wt% ErCuX (hexagonal $P6/mmm$ or $P6_3/mmc$) impurity.

Magnetic characterization was carried out on a Quantum Design physical properties measurement system (PPMS) susceptometer/magnetometer at temperatures from 1.8 K to RT. AC susceptibility (χ_{ac}) measurements made with a driving field of 1 mT at 337 Hz are shown in figures 1–3. Both the stannide (figure 1) and the germanide (figure 2) show two clear peaks in χ' which we associate with the ordering of Er moments on the 2d and 4e sites. The loss signal (χ'') for the stannide shows an additional feature at ~2.2 K which might be associated with the change in magnetic scattering reported below 3 K in $Er_3Cu_4Sn_4$ [1]. Data on the silicide (figure 3) are dominated by the event at 3.3 K which we again associate with the Er 4e ordering; however, the upper transition is less evident and only shows as a weak departure from Curie–Weiss behaviour. Subtraction of this $1/T$ background yields a clear peak at 13.8 K which we associate with the Er 2d ordering. χ'' also shows a peak at 3.3 K corresponding to the ordering of the Er 4e moments. In all three alloys, χ'' shows little or no change at the upper transition (Er 2d ordering) but a clear peak is seen at the Er 4e
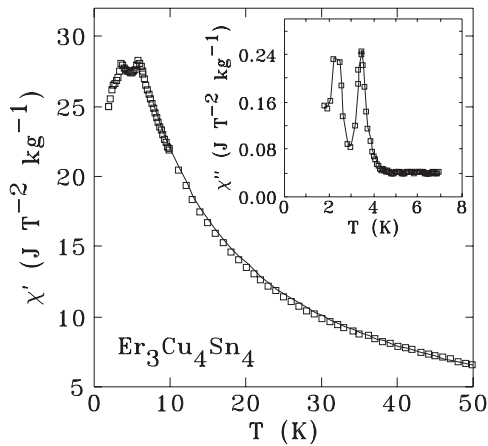
Figure 1. Temperature dependence of the ac susceptibility (χ') for Er$_3$Cu$_4$Sn$_4$ showing features at 3.6 and 5.8 K. The solid curve is a Curie–Weiss fit. The inset gives the out of phase (loss) response (χ'') which reveals an additional feature at 2.2 K.
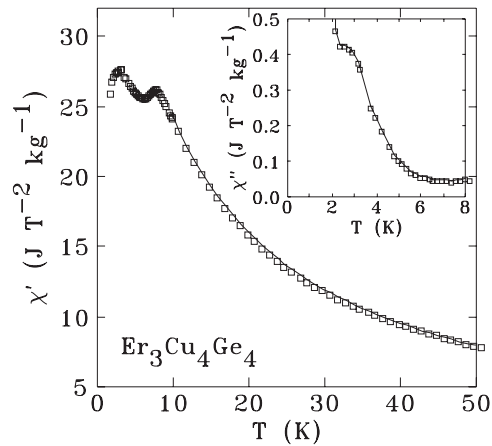
Figure 2. Temperature dependence of the ac susceptibility (χ') for Er$_3$Cu$_4$Ge$_4$ showing features at 3.2 and 7.9 K. The solid curve is a Curie–Weiss fit. The inset gives the out of phase (loss) response (χ'') which shows a weak shoulder at $\sim$3 K.
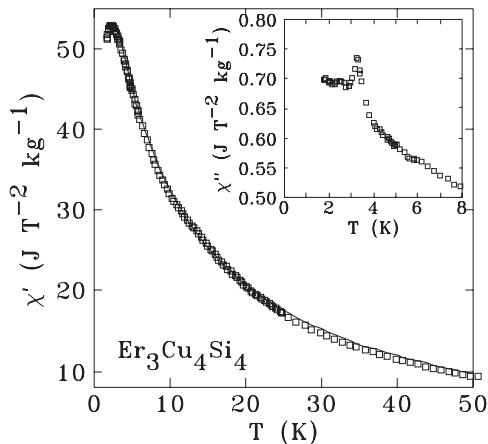
Figure 3. Temperature dependence of the ac susceptibility (χ') for Er$_3$Cu$_4$Si$_4$ showing a peak at 3.3 K as the Er 4e moments order. The solid curve above 30 K is a Curie–Weiss fit. The inset gives the out of phase (loss) response (χ'') which also shows the 3.3 K Er 4e ordering event. The ordering of the Er 2d moments at 13.8 K shows only as a weak deviation from Curie–Weiss behaviour in the $\chi'(T)$ curve.
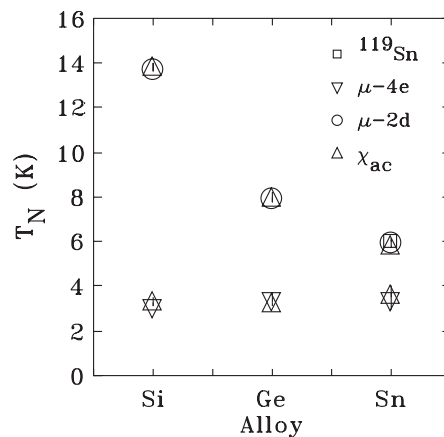
Figure 4. Transition temperatures for Er$_3$Cu$_4$X$_4$. $\chi_{ac}(T)$ data show two peaks as Er moments on the two sites order ($\triangle$). These peaks correspond well with ordering on the two sites detected by neutron scattering (Sn [1], Ge [3] and Si (this work)). The onset of magnetic splitting in the ^{119}Sn Mössbauer spectra reveals only a single transition in Er$_3$Cu$_4$Sn$_4$ ($\square$). Errors are small and are shown as bars within the plotted points.

ordering temperature. The metalloid dependence of the two transition temperatures is shown in figure 4. While the ordering temperature of the Er 2d moments clearly falls rapidly as we move from Si to Sn, the behaviour of the Er 4e moments is virtually unchanged. The high-temperature sections of $\chi'(T)$ could be fitted to a Curie–Weiss law ($\chi = C/(T - \theta_p)$, see table 1 for fitted values) yielding negative Curie–Weiss temperatures (θ_p) as expected for these antiferromagnetic alloys, but the effective moments are somewhat larger than the 9.58 μ_B
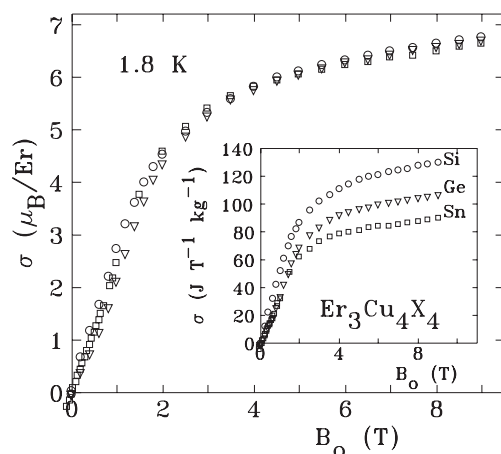
Figure 5. Magnetization curves for $Er_3Cu_4X_4$ at 1.8 K showing that the alloy moments are substantial, and essentially identical. The inset shows the mass-normalized data at the same temperature.

expected for Er; however, these values are not out of line with results for Er_3Ge_4 [6], $ErGe_2$ [9] and $ErGe_3$ [10].

Magnetization measurements made in fields of up to 9 T at 1.8 K are shown for all three alloys in figure 5. Two things are immediately apparent:

 (i) all three alloys are essentially identical once the changing formula weight is accounted for;
 (ii) the observed magnetization at 9 T is far larger than would be expected from the Er moments derived from neutron scattering.

The anisotropy is clearly small, and the weak exchange indicated by the small Curie–Weiss temperatures, coupled with the large Er moments, make it possible for the 9 T applied field to fold up the antiferromagnetic spin structure and almost saturate the magnetization. Arrott plots for the temperature region around the Er 2d ordering temperature show no evidence of a ferromagnetic component to the magnetic ordering in any of the materials, confirming that the order is entirely antiferromagnetic. The average Er moment in all three of these alloys observed at 1.8 K in 9 T is 6.72(4) μ_B, far larger than the average value found by neutron diffraction at 1.5 K in the stannide (3.5(3) μ_B [1]), the germanide (5.1(2) μ_B [3]) or the silicide (3.9(3) μ_B (this work)). The incomplete saturation apparent in figure 5 would suggest that the actual average Er moment is even larger than 6.72(4) μ_B.

3. Mössbauer spectroscopy

3.1. ^{119}Sn data

^{119}Sn Mössbauer spectra were obtained using a 370 MBq ^{119m}SnBaSnO$_3$ source. Typical linewidths were 0.51 mm s^{-1} (HWHM). Low temperatures were obtained using a helium-flow cryostat with the source at ambient temperature. The spectrometer was operated in constant-acceleration mode and calibrated against a 99.99% α-Fe foil using a ^{57}Co source. Spectra were fitted using a non-linear least-squares minimization routine with line positions and intensities derived from a full solution to the nuclear Hamiltonian. A free fit to two sites at
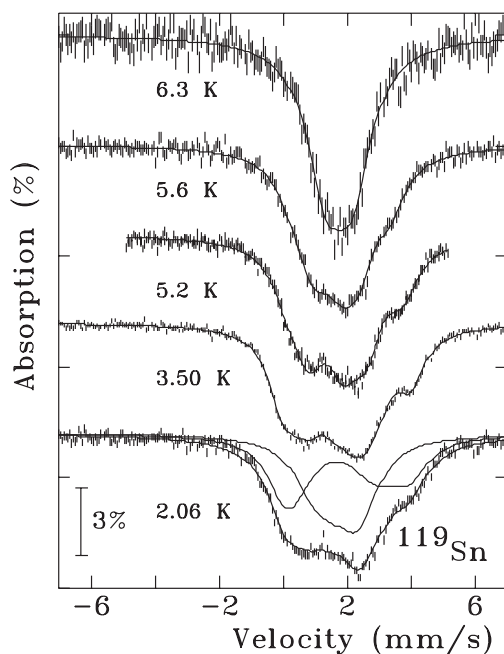
Figure 6. ^{119}Sn Mössbauer spectra of Er$_3$Cu$_4$Sn$_4$ taken at temperatures through T_N. Two equal-area magnetically split contributions (one from each of the two Sn sites) are distinguishable and are shown at 2.06 K. Solid curves are fits using a static Hamiltonian.

Table 2. First-neighbour Er environments of the two Sn sites in Er$_3$Cu$_4$Sn$_4$ used for transferred field calculations.

Tin site	Er neighbours		Distance (Å)
	Number	Type	
4f	1	2d	3.063
	2	4e	3.139
	2	4e	3.630
4h	2	2d	3.083
	4	4e	3.376

2 K gave areas of 45(3)%:55(3)%. For the final fits, two equal-area contributions, as demanded by the crystal structure, were used.

The spectra shown in figure 6 clearly exhibit an increasing magnetic splitting on cooling. As the Sn atom has no local moment, any magnetic hyperfine field observed in a ^{119}Sn Mössbauer spectrum must be due to the effects of moments on neighbouring atoms. The environments of the two Sn sites in Er$_3$Cu$_4$Sn$_4$ calculated from the known crystal structure using the BLOKJE program [11] are given in table 2. Both Sn sites have Er 2d and Er 4e atoms as neighbours and should therefore be sensitive to changes in the magnetic order at both Er sites. However, the temperature dependence of the hyperfine field shown in figure 7 provides evidence for only a single magnetic transition at 6 K, i.e. that associated with the ordering of the Er 2d moments. There is no apparent change at the 3.6 K ordering of the Er 4e moments, despite the fact that both Sn sites have four Er 4e first neighbours.
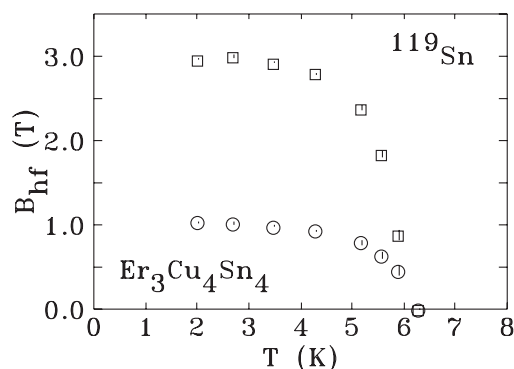
Figure 7. Temperature dependence of the ^{119}Sn hyperfine fields at the two Sn sites (Sn 4h □, Sn 4f ○) in Er$_3$Cu$_4$Sn$_4$. Note: only a single transition at ∼6 K is apparent; there is no effect due to the ordering of the Er 4e sublattice at 3.6 K. Errors are small and are shown as bars within the plotted points.

The very different fields observed at the two Sn sites permit a tentative identification of the two components. Given the absence of a change at 3.6 K, we assume no transferred hyperfine field from the Er 4e sublattice. This approximation is somewhat consistent with the much smaller moments reported at this site [1] and also with the poor degree of ordering on the Er 4e sites at these temperatures inferred from our neutron scattering data discussed below. With only one Er 2d neighbour, the Sn 4f will see a transferred field in the ordered state, independent of the actual magnetic structure. The Sn 4h has two Er 2d neighbours at $(0, \frac{1}{2}, 0)$ and $(0, \frac{1}{2}, 1)$, i.e. at the same a and b, but displaced above and below along c. Since the propagation vector for the Er 2d ordering is $[\frac{1}{2}\frac{1}{2}0]$ [1], there is no doubling along c and the two neighbouring Er 2d moments should be parallel. The Sn–Er distances are all essentially the same for the two Sn sites, so this leads us to expect the field at the Sn 4h to be about twice that seen at the Sn 4f. A factor of nearly three is apparent in figure 7. We therefore assign the larger-field site to Sn 4h.

The absence of a change in ^{119}Sn hyperfine field as the Er 4e moments order at 3.6 K in this alloy suggests that either the Er 4e moments are very small (contradicted by our ^{166}Er Mössbauer data below), or that the moment correlations are short ranged and that the ordering is very far from complete even at 2 K.

3.2. ^{166}Er data

^{166}Er Mössbauer measurements were carried out using 1 GBq ^{166}Ho sources prepared by neutron activation of Ho$_{0.6}$Y$_{0.4}$H$_2$ in the SLOWPOKE reactor at Ecole Polytechnique, Montréal. This spectrometer was operated vertically with both source and sample cooled in a helium-flow cryostat and gave a linewidth of 2.5 mm s^{-1} (HWHM) for an ErFe$_2$ standard at 4.5 K. Independent temperature control of the source was used to keep it at or above 5 K to avoid relaxation-induced line broadening which we have observed at lower source temperatures. A He/Ne laser interferometer was used to provide simultaneous calibration of all spectra. With the spectrometer operated in sine mode, at a V_{max} of ∼82 mm s^{-1}, the calibration drift in V_{max} was less than 0.02 mm s^{-1}. Velocity calibration was cross-checked against both 99.99% α-Fe at lower velocities to confirm linearity, and ErFe$_2$ [12] at our operating velocity. Reproducibility was better than 0.1%.
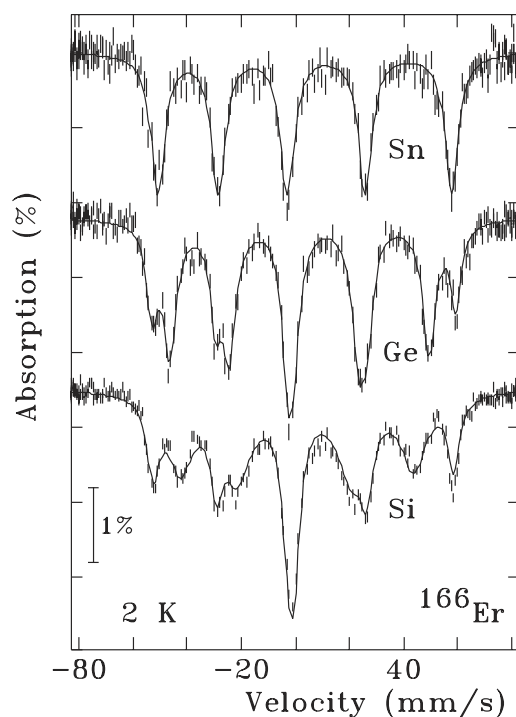
Figure 8. ^{166}Er Mössbauer spectra of Er$_3$Cu$_4$X$_4$ at 2 K. The 4e and 2d contributions become less distinct as we move from Si to Sn. Only a single Er site is apparent for the stannide.

The spectra at 2 K (figure 8) were fitted using a conventional non-linear least-squares minimization routine with line positions and intensities derived from a full solution to the nuclear Hamiltonian for the ^{166}Er 2 → 0 transition.

The hyperfine field at the Er nucleus is directly proportional to the moment on the Er atom. The free-ion hyperfine field corresponding to a moment of 9 μ_B on Er is 770.5 ± 10.5 T [13]. There will be an additional contribution of ∼14.1 ± 2.1 T from parent conduction electron polarization [14] in a metallic environment, giving a total field of 784.6 ± 10.7 T and a moment to field conversion factor of 87.2 ± 1.2 T/μ_B. We have previously shown that this factor works well in Er$_3$Ge$_4$ [6]. In addition, the relative areas in a Mössbauer spectrum are related to the crystallographic multiplicities of the sites yielding each component, so that the areas, if unique, can be used to identify the origin of each component. Therefore, ^{166}Er Mössbauer spectroscopy provides a direct measure of the moment on each Er site, and as the areas are in a 2:1 ratio the components in the spectra can be assigned unambiguously to the two sites in the Er$_3$Cu$_4$X$_4$ structure.

Examination of the spectra in figure 8 leads immediately to the conclusion that the moment on the Er 2d site is indeed larger than that on the Er 4e (the wider split pentet has a smaller area than the narrower one) but only by at most 30%. Furthermore, the Mössbauer data provide no evidence for distinct Er moments in Er$_3$Cu$_4$Sn$_4$. The fitted hyperfine fields are plotted with the neutron diffraction moments in figure 9. For both the silicide and germanide we see excellent agreement between the Mössbauer and neutron diffraction moments at the Er 2d site; however, this does not carry over to the stannide where the neutron moment is only 80% of that determined by ^{166}Er Mössbauer spectroscopy. The situation at the Er 4e site is far worse, with
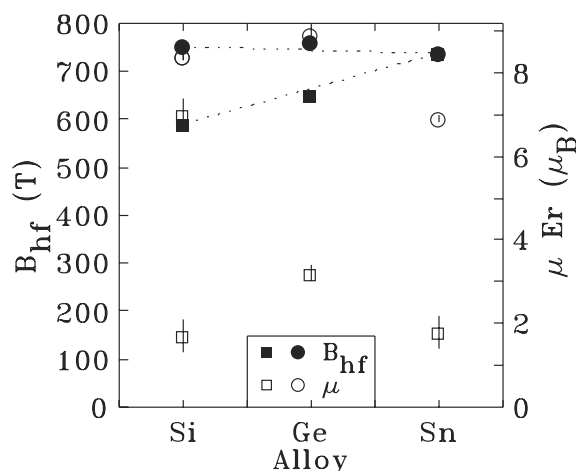
Figure 9. Er moments at the 4e and 2d sites derived from ^{166}Er Mössbauer spectroscopy (2 K, solid symbols) and neutron diffraction (open symbols). Circles: Er 2c site. Squares: Er 4e site. Neutron data for Sn (1.5 K, [1]), Ge (1.5 K, [3]) and Si (2.4 K, this work). Errors are shown as vertical bars.

disagreements close to a factor of three. Average Er moments derived from ^{166}Er Mössbauer spectroscopy for the three alloys are 7.31 μ_B (Si), 7.88 μ_B (Ge) and 8.46 μ_B (Sn), which are all greater than the lower limit of 6.72(4) μ_B set by the magnetization data. By contrast, neutron diffraction gives 3.9(3) μ_B (Si, this work), 5.1(2) μ_B (Ge) [3] and 3.5(3) μ_B (Sn) [1], all of which are well below the 6.72(4) μ_B lower limit set by magnetization. It seems likely that the neutron diffraction is leading to a severe underestimate of the erbium moments.

Slow electronic relaxation effects are ubiquitous in ^{166}Er Mössbauer spectra, occurring in both oxides [15] and alloys [16]. The current alloys are no exceptions, with the lines broadening and collapsing towards the centre with increasing temperature. The simplest way to formally include the effects of dynamics is to use a stochastic model [17] in which the hyperfine field at an Er site is assumed to fluctuate randomly between $\pm B_{hf}$ with some average effective frequency ν. While this model gives excellent fits to the data, it yields zero net magnetization and, strictly speaking, describes a slowly relaxing paramagnetic system. However, as we are only interested in tracking the onset of the relaxation behaviour, this model was considered adequate. The silicide showed the strongest effects of magnetic relaxation, with the Er 4e subspectrum visibly broadened even at 2 K (figure 10). Raising the temperature leads to a rapid increase in effective relaxation rate and the Er 4e subspectrum collapses into the centre, becoming little more than a broad background by 5 K. Similar, but less severe, relaxation is seen in the germanide (figure 11) with both components remaining distinct even at 10 K, above T_N. By contrast, the spectrum of the stannide (figure 12) evolves as a single unit; there is no evidence of a second component at any temperature that we investigated (figure 12 shows spectra up to 16 K, $\sim 2.7 \, T_N$). The effective relaxation rates, determined within our stochastic model, at the Er 4e sites are summarized in figure 13, where the earlier onset and much greater effective relaxation rates in the silicide are clearly seen. A simple linear fit to the relaxation rates suggests an onset temperature of 0.7(2) K for the silicide, while the stannide only starts above 2.5(2) K. Despite the ~ 1 GHz relaxation at the Er 4e site in the silicide at 8 K, the Er 2d component is essentially static. This extreme difference in relaxation behaviour at two Er sites in the same alloy was also observed in Er_3Ge_4 [6].
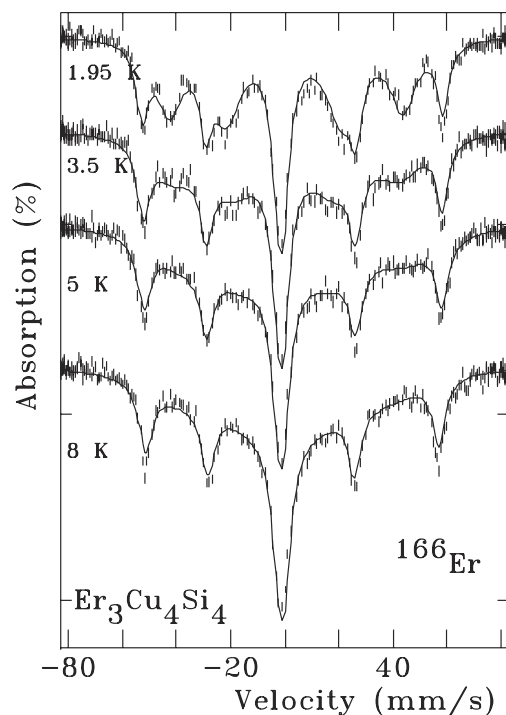
Figure 10. ^{166}Er Mössbauer spectra of Er$_3$Cu$_4$Si$_4$ taken at temperatures below T_N. The magnetic pentets from the two Er sites are clearly resolved, especially at 1.95 K. It is clear that the Er moments on the 4e site relax rapidly with increasing temperature, and this component is almost entirely washed out by 5 K. Solid curves are fits to two sites using a dynamic relaxation model.

At the lowest temperatures this slow electronic relaxation works to our advantage as it suppresses any possible dynamic effects and permits the ^{166}Er Mössbauer measurement to access the total, static Er moment at each site. The derived values are also independent of any short-range correlations as the hyperfine field is dominated by the effects of the local Er moment. The excellent agreement with neutron diffraction data for both Er sites in Er$_3$Ge$_4$ [6], and the clear consistency seen here in all three alloys for the Er moment at the Er 2d site, supports this interpretation. We therefore conclude from the ^{166}Er Mössbauer data that the average Er moment on the 2d sites in this system is 8.61(8) μ_B, and that the Er 4e moment decreases as we move from Sn to Si, but is never less than 6.72(4) μ_B.

4. Neutron diffraction

Given the clear disagreement between the neutron diffraction moments on the one hand, and the ^{166}Er Mössbauer spectra and bulk magnetization data on the other, we felt that the neutron diffraction measurements should be re-evaluated. Data on the germanide [3] and stannide [1] are already available; furthermore, it is clear from figure 4 that the silicide has the largest gap between the ordering temperatures of the two Er sublattices and so offers the cleanest access to the lower transition as the ordering of the Er 2d sublattice should be well established before any changes start at the Er 4e sublattice. We therefore selected the silicide for further study.

Neutron powder diffraction experiments on Er$_3$Cu$_4$Si$_4$ were carried out on a ~5 g sample on the DUALSPEC C2 high-resolution powder diffractometer [18] located at the NRU reactor,
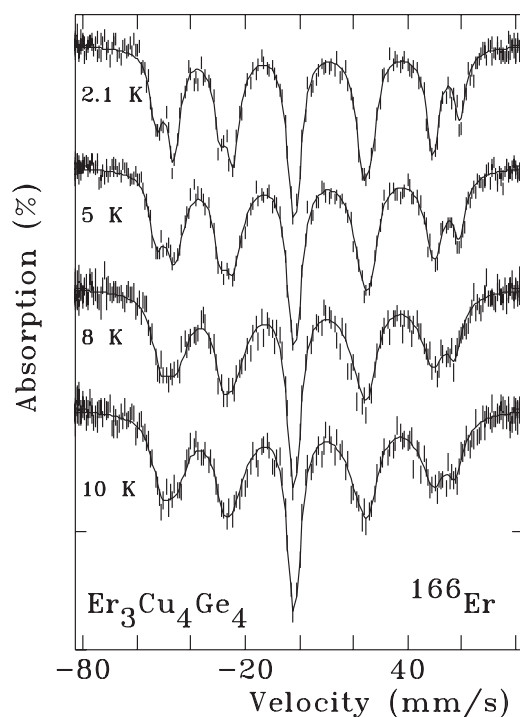
Figure 11. [166]Er Mössbauer spectra of $Er_3Cu_4Ge_4$ taken at temperatures either side of T_N (=8 K). The magnetic pentets from the two Er sites are clearly resolved, especially at 2.1 K. Relaxation effects are apparent at both sites. Solid curves are fits to two sites using a dynamic relaxation model.

Chalk River Laboratories, operated by Atomic Energy Canada Ltd. The neutron wavelength was 2.3685(1) Å. Temperatures down to 2.4 K were achieved using an 'orange'-type He-flow cryostat. All diffraction patterns were analysed using the Rietveld method with the FULLPROF program [19]. The symmetry related restrictions placed on the allowed magnetic structures of the Er sublattices in $Er_3Cu_4Si_4$ were checked using the SARA*h* representational analysis program of Wills [20].

The annealed sample of $Er_3Cu_4Si_4$ was virtually single phase, with a trace (<2 wt%) of ErCuSi present, as determined from fits to the neutron diffraction patterns. ErCuSi can form in two related hexagonal structures with the space groups $P6_3/mmc$ and $P6/mmm$. Our impurity phase appears to be the latter. FULLPROF refinement of the non-magnetic diffraction pattern at 20 K (figure 14, top panel) was used to determine structural parameters. The crystal structure of $Er_3Cu_4Si_4$ is orthorhombic with the space group $Immm$ (No. 71) [8]. There are two Er sites (2d and 4e), one Cu site (8n) and two Si sites (4f and 4h). The lattice parameters for $Er_3Cu_4Si_4$ at 20 K were found to be $a = 13.5581(5)$ Å, $b = 6.4974(2)$ Å and $c = 4.0886(2)$ Å. The conventional refinement R-factors (%) for the 20 K pattern are $R(\text{Bragg}) = 4.7$ and $R(F - \text{struct.}) = 5.9$. During the neutron diffraction fitting procedure we employed three refinable isotropic thermal parameters (B_{iso}), one for each element. The refined atomic positions and isotropic thermal parameters are given in table 3.

At 6 K, only the Er 2d moments are ordered in $Er_3Cu_4Si_4$. We obtained the best fit to the 6 K neutron diffraction pattern (figure 14, centre panel) with the Er 2d moments placed along the [001] direction with a propagation vector $[0\frac{1}{2}0]$. This ordering is the same as that observed
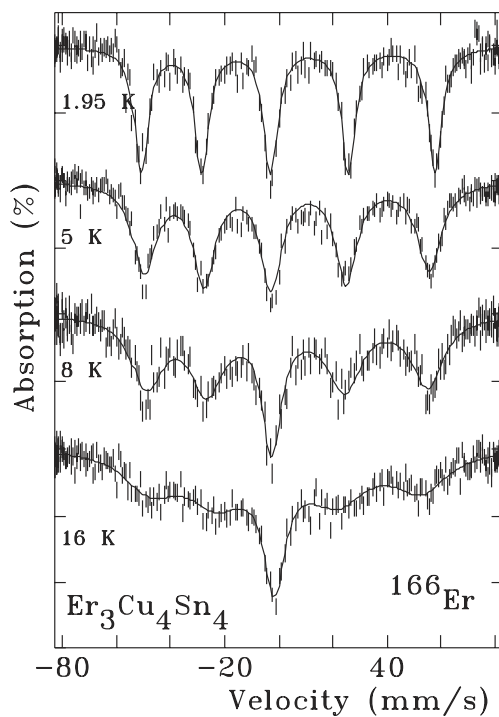
Figure 12. ^{166}Er Mössbauer spectra of $Er_3Cu_4Sn_4$ taken at temperatures either side of T_N (=6 K). Only a single contribution is visible at any temperature. Solid curves are fits using a dynamic relaxation model.
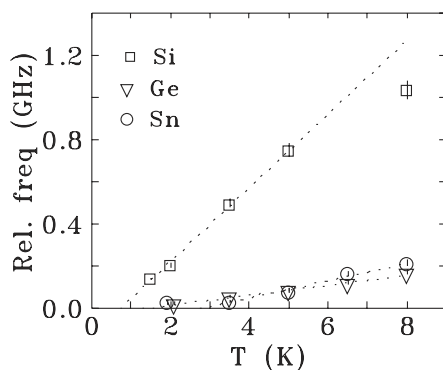

Figure 13. Temperature dependence of the ^{166}Er hyperfine field relaxation rates at the 4e site in $Er_3Cu_4X_4$. Relaxation persists to lower temperatures in the silicide. Dotted curves are guides to the eye. Errors are small and are shown as bars within the plotted points.

in $Er_3Cu_4Ge_4$ by Wawrzyńska *et al* [3]. The magnetic structure of the Er 2d sublattice is straightforward—an antiferromagnetic structure doubled along the crystal *b*-axis [010] with the moments ordering along the *c*-axis [001]. The refined Er 2d magnetic moment at 6 K is 8.3(1) μ_B. Representation analysis for the Er 2d site, with a propagation vector $[0\frac{1}{2}0]$, shows that the decomposition of the magnetic representation involves three one-dimensional
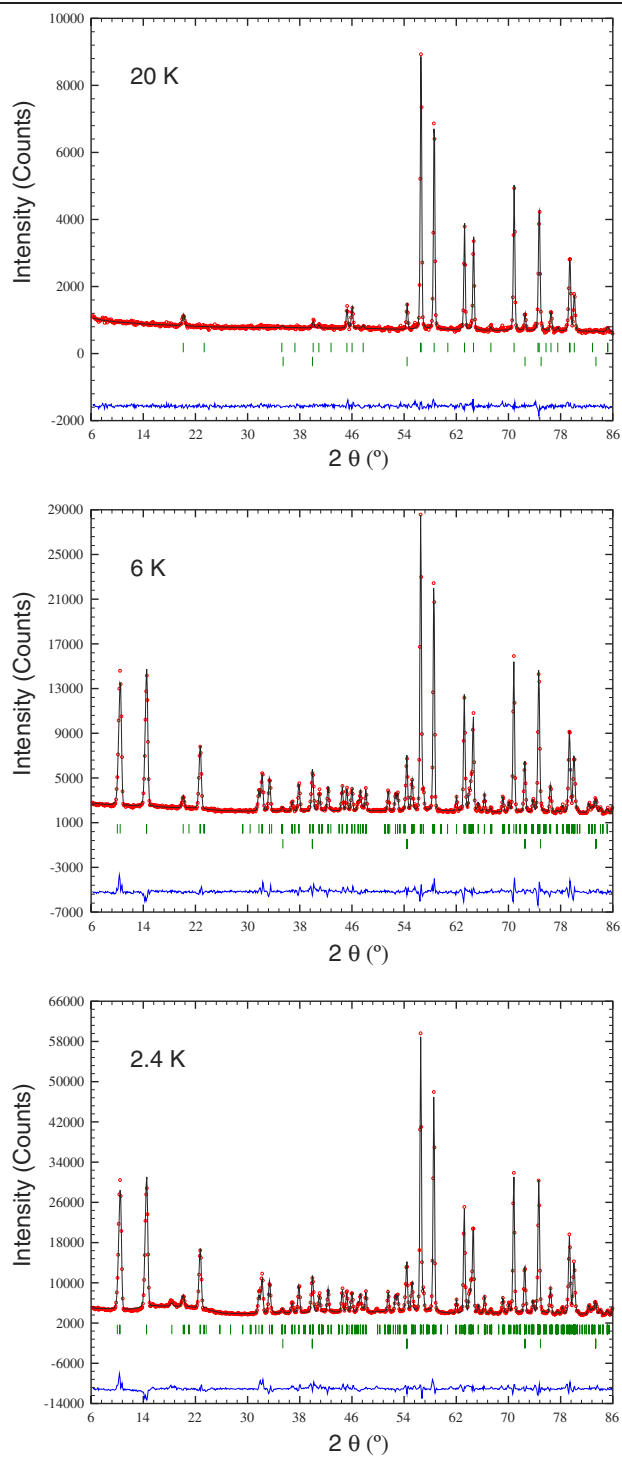
Figure 14. Neutron diffraction pattern for $Er_3Cu_4Si_4$ at top, 20 K; middle, 6 K, and bottom, 2.4 K. In each case the data with fit are shown at the top, Bragg markers for $Er_3Cu_4Si_4$ (upper set) and the ErCuSi impurity phase (lower set) are shown in the middle, and residuals are shown at the bottom.

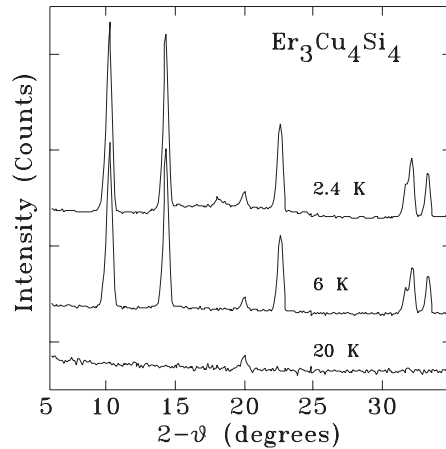(This figure is in colour only in the electronic version)

Figure 15. Low-angle sections of neutron diffraction patterns for $Er_3Cu_4Si_4$ in the non-magnetic state (20 K), below T_N for the 2d site (6 K), and below T_N for the 4e site (2.4 K). Only the weak peak at $\sim 18°$ marks the ordering of the Er 4e site moments.

Table 3. Atomic positions and isotropic thermal parameters (B_{iso}) for $Er_3Cu_4Si_4$ determined from neutron diffraction data at 20 K.

Atom	Site	x	y	z	B_{iso} (Å^2)
Er	2d	$\frac{1}{2}$	0	$\frac{1}{2}$	0.7(2)
Er	4e	0.1301(4)	0	0	0.7(2)
Cu	8n	0.3301(2)	0.1924(5)	0	0.4(1)
Si	4f	0.2200(8)	$\frac{1}{2}$	0	1.1(3)
Si	4h	0	0.1870(13)	$\frac{1}{2}$	1.1(3)

irreducible representations:

$$\Gamma_{Mag} = 1\Gamma_2^{(1)} + 1\Gamma_3^{(1)} + 1\Gamma_4^{(1)} \tag{1}$$

using the notation employed in the program SARA*h* [20]. The basis vectors of the irreducible representations are given in table 4. The magnetic structure of the Er 2d sublattice in $Er_3Cu_4Si_4$ at 6 K corresponds to the basis vector ψ_3 belonging to the $\Gamma_4^{(1)}$ irreducible representation.

Further cooling to 2.4 K leads to changes in the diffraction pattern associated with ordering on the Er 4e sites in addition to the ordered Er 2d moments (figure 14, bottom panel). The development of order on the Er 4e sites is demonstrated by the appearance of a number of small magnetic peaks, in particular one at $2\theta = 18°$ (figure 15). The Er 2d sublattice order is basically unaffected by the ordering of the Er 4e sublattice, this latter order being incommensurate with the lattice. At 2.4 K, the refined Er 2d moment increases slightly to 8.4(1) μ_B, while the refined Er 4e moment is far smaller, being only 1.7(4) μ_B. The incommensurate order of the Er 4e sublattice is characterized by ordering along [100] with a propagation vector of [0 0.876(5) 0]. Representation analysis for the Er 4e site, with a propagation vector [0 0.876(5) 0], shows that the decomposition of the magnetic representation involves four one-dimensional irreducible representations:

$$\Gamma_{Mag} = 1\Gamma_1^{(1)} + 2\Gamma_2^{(1)} + 2\Gamma_3^{(1)} + 1\Gamma_4^{(1)}. \tag{2}$$

The basis vectors of the irreducible representations are given in table 5. The best fit to the Er 4e sublattice order corresponds to the basis vector ψ_4 belonging to the $\Gamma_3^{(1)}$ irreducible representation.

Table 4. Representation analysis for the Er 2d site in $Er_3Cu_4Si_4$ with a propagation vector $[0\frac{1}{2}0]$. The atomic position of the primitive basis is $(\frac{1}{2},0,\frac{1}{2})$.

Representation	Basis vector	Atom 1
$\Gamma_2^{(1)}$	ψ_1	[010]
$\Gamma_3^{(1)}$	ψ_2	[100]
$\Gamma_4^{(1)}$	ψ_3	[001]

Table 5. Representation analysis for the Er 4e site in $Er_3Cu_4Si_4$ with a propagation vector $[0\ 0.876(5)\ 0]$. The atomic positions defining the non-primitive basis are $(x, 0, 0)$ and $(-x, 0, 0)$.

Representation	Basis vector	Atom 1	Atom 2
$\Gamma_1^{(1)}$	ψ_1	[001]	[00$\bar{1}$]
$\Gamma_2^{(1)}$	ψ_2	[100]	[$\bar{1}$00]
$\Gamma_2^{(1)}$	ψ_3	[010]	[010]
$\Gamma_3^{(1)}$	ψ_4	[100]	[100]
$\Gamma_3^{(1)}$	ψ_5	[010]	[0$\bar{1}$0]
$\Gamma_4^{(1)}$	ψ_6	[001]	[001]

The temperature dependences of the first four magnetic reflections from $Er_3Cu_4Si_4$ are shown, with their indices, in figure 16. Two distinct ordering events are clearly visible. The onset temperatures are plotted along with those of the germanide [3] and stannide [1] in figure 4 and are in complete agreement with transition temperatures determined by χ_{ac}.

One question remains concerning the magnetic structure of the Er 4e moments. Wawrzyńska *et al* [1, 3] described it as a sine-modulated antiferromagnet, propagating along the *b*-axis with the direction of magnetic order along the *a*-axis. However, such a structure implies a distribution of Er^{3+} magnetic moments, which is inconsistent with our ^{166}Er Mössbauer spectrum obtained at 1.95 K (figure 10) where we observe a single, large and sharp magnetic hyperfine field at the Er 4e sites and hence a single, well defined, and large Er^{3+} moment. Furthermore, it is unlikely that the Er^{3+} structure is helical or spiral because orthorhombic groups do not have two-dimensional irreducible representations. While such structures are not impossible in orthorhombic groups [21], and they can arise due to accidental degeneracies in the order parameters, they are rare. A possible magnetic structure for the Er 4e sublattice that is consistent with both our neutron diffraction data and the ^{166}Er Mössbauer spectrum is a square-wave modulated antiferromagnet. This would yield a single Er moment (and hence hyperfine field) and would also require a propagation vector. If the 4e sublattice does indeed order as a square-wave modulated antiferromagnet one would expect to observe higher-order, odd harmonics of the propagation vector $[0\ 0.876(5)\ 0]$. Unfortunately, the extremely low intensity of the first-order harmonic which is the 000_{4e}^+ peak at $2\theta \sim 18°$ renders the weaker, higher-order harmonics virtually impossible to locate.

Thus far, our analysis matches that done earlier [1, 3], and we observe the same anomalously small Er 4e moment that is in severe disagreement with that seen by ^{166}Er Mössbauer spectroscopy. However, closer examination of the 2.4 K diffraction pattern reveals a broad feature in the range $10° < 2\theta < 30°$, that only develops as the ordering of the Er 4e starts to appear. Figure 17 shows the result of subtracting the diffraction pattern obtained at 6 K from that at 2.4 K in order to emphasize the changes associated with the Er 4e ordering. It clearly shows the form of this previously unreported feature. Furthermore, careful examination
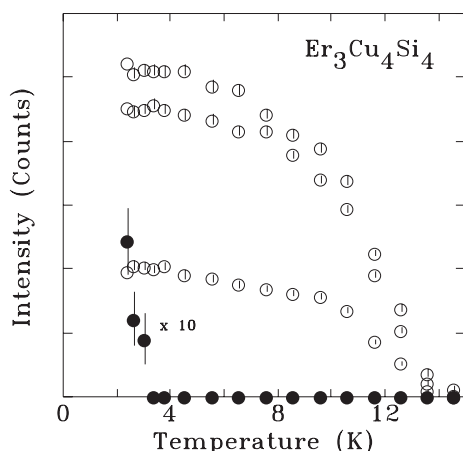
Figure 16. Temperature dependence of the first four magnetic diffraction peaks in the neutron scattering patterns of $Er_3Cu_4Si_4$. Open symbols derive from ordering of the Er 2d sublattice: (top to bottom) $010^-_{2d}/110^+_{4e}$ at $\sim 10°$, 100^+_{2d} at $\sim 15°$ and $210^-_{2d}/110/020^+_{4e}$ at $\sim 22°$. Solid symbols: 000^+_{4e} peak at $\sim 18°$ deriving from ordering of the Er 4e sublattice (scaled by a factor of ten). Two distinct onsets are clearly visible. Errors are mostly small and appear as bars within the plotted points.
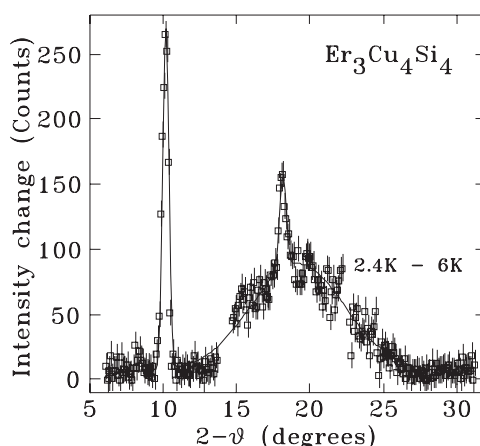
Figure 17. Difference between the diffraction patterns obtained at 2.4 and 6 K for $Er_3Cu_4Si_4$ emphasizing the broad feature that develops as the Er 4e moments start to order. The peaks at $\sim 15°$ and $\sim 22°$ were deleted to make the form of the broad feature more prominent. The solid curve is a fit using three Gaussian peaks.

of the same region of the published diffraction data on the germanide (see figure 8 of [3]) and the stannide (see figure 9 of [1]) reveals that the same broad feature is present in the low-temperature diffraction patterns of both systems, and that it was treated as a background contribution, much as we have done in figure 14 at 2.4 K. Fitting the difference plot in figure 17 as a sum of Gaussians allows us to estimate the area of the broad feature. If we normalize it to the area of the 000^+_{4e} peak associated with the ordering of the Er 4e sublattice we obtain an area ratio of $1:16.9 \pm 1.7$. If we further assume that all of this broad scattering is associated with Er 4e moments and that the area of this feature, along with that of the 000^+_{4e} peak, represents the total scattering from the Er 4e moment at this wavevector, we can scale our fitted Er 4e moment ($1.7(4)$ μ_B) to obtain a revised estimate for the zero-temperature Er 4e moment of 7.2 ± 1.7 μ_B. This value is consistent with the $6.76(1)$ μ_B that we derive from our ^{166}Er Mössbauer data. Furthermore, the width of this broad feature leads to an estimate of ~ 40 Å for the effective Scherrer 'particle' size, and hence a correlation radius of ~ 20 Å for the Er 4e spins at 2.4 K. The feature seen here in the silicide is very similar in form to the ones seen in both the germanide [3] and stannide [1], so that our failure to detect the ordering of the Er 4e moments at 2 K in $Er_3Cu_4Sn_4$ using ^{119}Sn Mössbauer spectroscopy is probably due to the incomplete and poorly correlated ordering that occurs on the Er 4e sites at these temperatures.

5. Conclusions

Neutron diffraction on $Er_3Cu_4Si_4$ confirms the previously reported distinct ordering temperatures of erbium moments on the 2d and 4e sites in $R_3Cu_4X_4$ (X = Ge, Sn). However, we find that the ordering of the Er 4e moments in all three compounds is incomplete by 2.4 K with

correlation lengths of only ∼20 Å. While our neutron diffraction data yield a severely reduced Er moment on the 4e site, the incomplete ordering and short correlation length inevitably leads to this significant underestimate. ^{166}Er Mössbauer spectroscopy for $R_3Cu_4X_4$ (X = Si, Ge, Sn) provides a better measure of the Er moments on both sites and confirms that Er 4e moments are indeed smaller, but only by about 30%, not the factor of three previously claimed.

Acknowledgments

References

[1] Wawrzyńska E, Hernandez-Velasco J, Penc B, Sikora W, Szytula A and Zygmunt A 2003 *J. Phys.: Condens. Matter* **15** 5279
[2] Szytula A, Wawrzyńska E, Penc B, Stüsser N and Zygmunt A 2003 *Physica* B **327** 167
[3] Wawrzyńska E, Hernandez-Velasco J, Penc B, Szytula A and Zygmunt A 2003 *J. Magn. Magn. Mater.* **264** 192
[4] Wawrzyńska E, Penc B, Stüsser N, Szytula A and Tomkowicz Z 2003 *Solid State Commun.* **126** 527
[5] Zaharko O, Keller L and Ritter C 2002 *J. Magn. Magn. Mater.* **253** 130
[6] Ryan D H, Cadogan J M and Gagnon R 2003 *Phys. Rev.* B **68** 014413
[7] Larson A C and von Dreele R B 2000 *Los Alamos National Laboratory Report* LAUR 86-748 (unpublished)
     Toby B H 2001 *J. Appl. Crystallogr.* **34** 210
[8] Hanel G and Nowotny H 1970 *Monatsh. Chem.* **101** 463
[9] Oleksyn O, Schobinger-Papamantellos P, Ritter C, de Groot C H and Buschow K H J 1997 *J. Alloys Compounds* **252** 53
[10] Schobinger-Papamantellos P, André G, Rodríguez-Carvajal J, de Groot C H and Buschow K H J 1996 *J. Alloys Compounds* **232** 165
[11] Gelato L 1982 *J. Appl. Crystallogr.* **14** 151
[12] Hodges J A, Jehanno G, Schuhl A and Berthier Y 1981 *Hyperfine Interact.* **11** 29
[13] Bleaney B 1988 *Handbook on the Physics and Chemistry of Rare Earths* vol 11, ed K A Gschneidner Jr and L Eyring (Amsterdam: Elsevier Science) chapter 77
[14] Li Y, Carboni C, Ross J W, McCausland M A H and Bunbury D St P 1996 *J. Phys.: Condens. Matter* **8** 865
[15] Nowik I and Wickman H H 1966 *Phys. Rev. Lett.* **17** 949
     Eibschütz M, Cohen R L and West K W 1969 *Phys. Rev.* **178** 572
[16] Wiedemann W and Zinn W 1967 *Phys. Lett.* A **24** 506
     Gubbens P C M, van der Kraan A M and Buschow K H J 1989 *Phys. Rev.* B **39** 12548
[17] Blume M and Tjon J A 1968 *Phys. Rev.* **165** 446
[18] Powell B M 1990 *Neutron News* **1** 16
[19] Rodríguez-Carvajal J 1993 *Physica* B **192** 55
[20] Wills A S 2000 *Physica* B **276–278** 680
[21] Rossat-Mignod J 1987 *Neutron Scattering* (*Methods of Experimental Physics* vol 23) ed K Sköld and D L Price (New York: Academic) chapter 19, pp 69–157